Improved Mass Measurements of Nuclei Around N=Z=34 for X-ray Burst Models

Joshua Savory[*][a,b], **C. Bachelet**[a], **M. Block**[a], **G. Bollen**[a,b], **M. Facina**[a], **C.M. Folden III**[a], **C. Guénaut**[a], **E. Kwan**[a,b], **A.A. Kwiatkowski**[a], **D.J. Morrissey**[a,c], **G.K. Pang**[a,c], **A. Prinke**[a,b], **R. Ringle**[a,b], **H. Schatz**[a,b], **P. Schury**[a,b], **S. Schwarz**[a], **C.S. Sumithrarachchi**[a,c]

[a] *National Superconducting Cyclotron Laboratory, East Lansing, MI 48824, USA*

[b] *Department of Physics and Astronomy, East Lansing, MI 48824, USA*

[c] *Department of Chemistry, East Lansing, MI 48824, USA*

Mass measurements of N ≈ Z nuclei are important for the study of symmetries in nuclear structure, modeling of element synthesis in the rp-process, and fundamental interaction tests. High precision mass measurements of ^{68}Se, ^{70}Se, ^{70m}Br, and ^{71}Br were performed at the Low Energy Beam and Ion Trap Facility (LEBIT) [1, 2, 3, 4] by Penning trap mass spectrometry of thermalized rare isotopes produced by fast-beam fragmentation. The new Q-values obtained from this data and the (p,γ) reaction rates from [5] allowed new calculations of the reverse (γ,p) reaction rates through detailed balance. The impact of our new measurements was shown by varying the Q-values within their uncertainties, recalculating the reverse reaction rates, and running rp-process network calculations.

---

[*]Speaker.

1. Introduction

Type I X-ray bursts occur when a neutron star accretes matter from a companion star that is rich in hydrogen and helium. The burst starts when the hot CNO cycle is superseded by the rp-process [6, 7]. During the rp-process the excess hydrogen on the crust of the neutron star is burned via (p, γ) reactions. The proton captures proceed along an isotonic chain until a weakly proton bound or proton unbound nucleus is encountered. At this point an equilibrium develops between the proton capture and disintegration rates. The nucleus at which this occurs are known as the "waiting points" of the burst. Once a waiting point nuclide is encountered the burst can only proceed through a β-decay or a double proton capture. The time it takes for the burst to proceed beyond a waiting point nuclei, the effective lifetime, is determined by the half-life and the net proton capture rate. The effective lifetime of the waiting points strongly influences the time scale and the final mass distribution of a type I X-ray burst.

The important waiting point nuclei in the N $\approx$ Z $\approx$ 34 region are ^{64}Ge, ^{68}Se, and ^{72}Kr. These nuclei can pose a delay of up 120 s, which is comparable to the duration of the entire burst. Due to the relatively long effective lifetimes of these nuclei, their decay products strongly influence the neutron star's crustal composition and properties such as its thermal and electrical conductivity [8]. The effective lifetimes of these nuclei are also responsible for the long tails observed in the light curves of hydrogen rich type I X-ray bursts. In order to determine the effective lifetime of these nuclei, measurements of the associated masses, half-lives and proton capture rates are necessary. Most of the half-lives in the N $\approx$ Z $\approx$ 34 region have been measured to the desired accuracy; thus, reaction rates are the critical parameters. The necessary forward (p,γ) rates can be calculated by summing over the involved resonances, as shown in [9]. The reverse (γ, p) rates can be calculated, using the associated Q-values and the forward reaction rates, through detailed balance. Due to the exponential mass dependency of the reverse reaction rate calculations, mass measurements of the ground states on the order of 10 keV or less are necessary in order to keep the calculated uncertainty small.

In this paper, high-precision Penning trap mass measurements of ^{68}Se, ^{70}Se, ^{70m}Br and ^{71}Br are presented. In all cases the uncertainties in the existing mass values were improved by one to two orders of magnitude. The new data were used to improve rp-process network calculations.
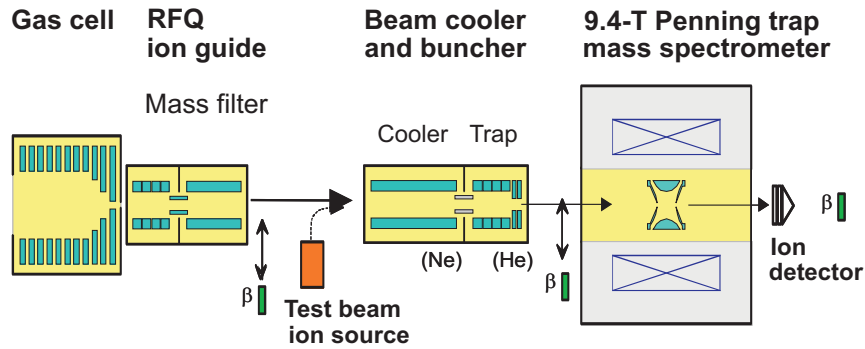
Figure 1: Schematic of the Gas Stopping Station and the LEBIT facility.

2. Apparatus and Procedure

The experiment was performed at the Low Energy Beam and Ion Trap Facility (LEBIT) [1, 4, 10] installed at the Coupled Cyclotron Facility of the NSCL at MSU. A schematic layout of LEBIT is shown in Figure 1. The main components are a gas cell, a radio frequency quadrupole (RFQ) ion guide system, a beam cooler and buncher, and a 9.4 Tesla Penning trap mass spectrometer. The LEBIT facility [11] was the first to demonstrate that fast radioactive beams from fragmentation reactions can be efficiently converted into low emittance pulsed beams and measured to high precision in a Penning trap mass spectrometer [3].

Separated projectile fragments are stopped in a gas cell after passing through a solid degrader system and a thin Be window [12]. The residual energy of the ions was removed by interaction with ultra-pure helium gas at a pressure $p = 0.3 - 1$ bar. The stopped ions were guided towards an extraction orifice with an electric field and finally swept out of the gas cell by the gas flow into a differentially pumped RFQ ion guide and mass filter system. After leaving the mass filter, which was typically operated with single mass resolving power, the ions were transported to a beam cooler and buncher. This system is based on a linear RFQ ion trap filled with a light buffer gas for ion cooling [13]. The ions were accumulated, cooled and then released as short ion pulses as required for efficient capture in the Penning trap. A fast electrostatic deflector in the beam transport line to the Penning trap was used as a time-of-flight mass filter. The high-precision Penning trap is located in the center of a $B = 9.4$ T superconducting solenoid. After capture, the ions were subjected to resonant dipole RF fields to remove possible impurities, exposed to a quadrupole RF field with a trial frequency at or close to ω_c for the cyclotron frequency determination, and then ejected. Their time of flight to an ion detector was measured in order to probe the radial energy gain due to this excitation. This cycle was repeated for different frequencies, and results in a resonance curve such as Figure 2 for ^{70}Se.
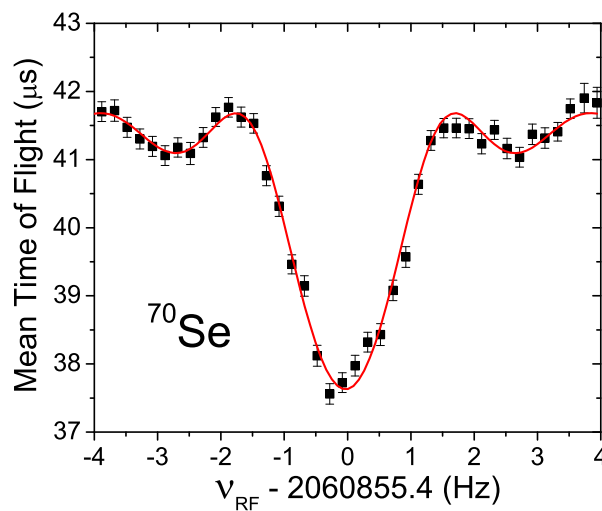
Figure 2: Cyclotron resonance obtained for ^{70}Se.
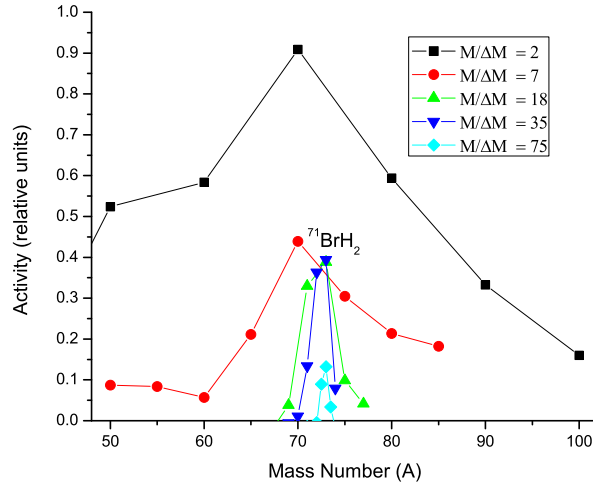
Figure 3: The observed activity vs mass number selected by the ion guide system for ^{71}Br using different mass filter resolving powers (M/ΔM).

In the present experiment a primary beam of ^{78}Kr with an energy of 150 MeV/u was impinged in a beryllium target to create a secondary beam of rare isotopes. The A1900 Fragment Separator selected the ions of interest by their magnetic rigidity. In order to stop and efficiently thermalize the ions the gas cell was operated at a helium gas pressure of 500 torr.

The Si detector located directly after the mass filter was used to identify the radioactive molecular adducts. A scan of the mass filter for ^{71}Br can be seen in Figure 3. The selenium ions were all extracted from the gas cell as atomic singly charged ions. The chemistry of the bromine ions differed depending on the level of ionization in the gas cell. For example, ^{71}Br was extracted from the gas cell as BrH_2^+; however due to the lower ionization level in the gas cell, ^{70}Br was extracted as Br^+.

3. Results

In addition to high-precision mass measurements of ^{68}Se, ^{70}Se, ^{70m}Br, and ^{71}Br, high accuracy mass predictions were made for ^{70}Kr and ^{71}Kr using the improved mass values for ^{70}Se and ^{71}Br, respectively, and Coulomb displacement energies from [14]. Using new mass values from this work, an earlier LEBIT data set [4], Coulomb displacement energies from [14], and forward (p,γ) reaction rates from [5], the reverse (γ,p) reaction rates were calculated by detailed balance. Next, all the Q-values in the N $\approx$ Z $\approx$ 34 region were varied within their uncertainties in order to determine the mass uncertainties in the reverse reaction rates. More precise information was obtained on the luminosity, nuclear generation rate, final elemental abundances, and temperature during a X-ray burst. Preliminary results for the nuclear energy generation rate are shown in Figure 4. More detailed results will be published later in [16].
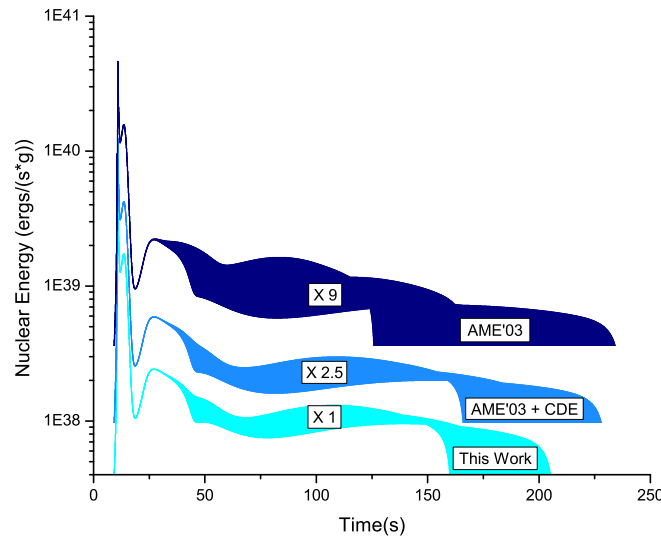
Figure 4: Nuclear energy generation rate as a function of time for a type I X-ray burst using the AME'03 [15], AME'03 and Coulomb displacement energies [14], and AME'03, Coulomb displacement energies [14], and the LEBIT data set. The different curves were scaled, by the given factor, and cropped in order to show an equal amount of each data set.

References

[1] M. Block et al., *Phys. Rev. Lett.* **100**, 132501 (2008).

[2] R. Ringle et al., *Phys. Rev. C* **75**, 055503 (2007).

[3] G. Bollen et al., *Phys. Rev. Lett.* **96**, 152501 (2006).

[4] P. Schury et al., *Phys. Rev. C* **75**, 055801 (2007).

[5] T. Rauscher and F.-K. Thielemann., *At. Dat. Nucl. Dat. Tab.* **75**, 1 (2000).

[6] R.K. Wallace and S.E. Woosley, *Astrophys. J. Suppl. Ser.* **45**, 389 (1981).

[7] H. Schatz and K.E. Rehm, *Nucl. Phys. A* **777**, 601 (2006).

[8] H. Schatz et al., *Phys. Rev. Lett.* **86**, 3471 (2000).

[9] W.A. Fowler and F. Hoyle, *Ap. J. Suppl.* **9**, 201 (1964).

[10] R. Ringle et al., *Int. J. Mass Spectrom.* **251**, 300 (2006).

[11] S. Schwarz et al., *Nucl. Instr. and Meth. B* **204**, 507 (2003).

[12] L. Weissman et al., *Nucl. Phys. A* **746**, 655c (2004).

[13] S. Schwarz et al., *Nucl. Instr. and Meth. B* **204**, 474 (2003).

[14] B. A. Brown et al., *Phys. Rev. C* **65**, 045802 (2002).

[15] A.H. Wapstra et al., *Nucl. Phys. A* **729**, 129 (2003).

[16] J. Savory et al., In Preparation.